OBSERVATION OF SINGLE ISOLATED ELECTRONS OF HIGH TRANSVERSE MOMENTUM IN EVENTS WITH MISSING TRANSVERSE ENERGY AT THE CERN p̄p COLLIDER

The UA2 Collaboration

M. BANNER [f], R. BATTISTON [1,2], Ph. BLOCH [f], F. BONAUDI [b], K. BORER [a], M. BORGHINI [b],
J.-C. CHOLLET [d], A.G. CLARK [b], C. CONTA [e], P. DARRIULAT [b], L. Di LELLA [b], J. DINES-HANSEN [c],
P.-A. DORSAZ [b], L. FAYARD [d], M. FRATERNALI [e], D. FROIDEVAUX [b], J.-M. GAILLARD [d],
O. GILDEMEISTER [b], V.G. GOGGI [e], H. GROTE [b], B. HAHN [a], H. HÄNNI [a], J.R. HANSEN [b],
P. HANSEN [c], T. HIMEL [b], V. HUNGERBÜHLER [b], P. JENNI [b], O. KOFOED-HANSEN [c],
E. LANÇON [f], M. LIVAN [b,e], S. LOUCATOS [f], B. MADSEN [c], P. MANI [a], B. MANSOULIÉ [f],
G.C. MANTOVANI [1], L. MAPELLI [b], B. MERKEL [d], M. MERMIKIDES [b], R. MØLLERUD [c],
B. NILSSON [c], C. ONIONS [b], G. PARROUR [b,d], F. PASTORE [b,e], H. PLOTHOW-BESCH [b,d],
M. POLVEREL [f], J.-P. REPELLIN [d], A. ROTHENBERG [b], A. ROUSSARIE [f], G. SAUVAGE [d],
J. SCHACHER [a], J.L. SIEGRIST [b], H.M. STEINER [b,3], G. STIMPFL [b], F. STOCKER [a], J. TEIGER [f],
V. VERCESI [e], A. WEIDBERG [b], H. ZACCONE [f] and W. ZELLER [a]

[a] Laboratorium für Hochenergie physik, Universität Bern, Sidlerstrasse 5, Bern, Switzerland
[b] CERN, 1211 Geneva 23, Switzerland
[c] Niels Bohr Institute, Blegdamsvej 17, Copenhagen, Denmark
[d] Laboratoire de l'Accélérateur Linéaire, Université de Paris-Sud, Orsay, France
[e] Dipartimento di Fisica Nucleare e Teorica, Università di Pavia and INFN, Sezione di Pavia, Via Bassi 6, Pavia, Italy
[f] Centre d'Etudes nucléaires de Saclay, France

We report the results of a search for single isolated electrons of high transverse momentum at the CERN p̄p collider. Above 15 GeV/c, four events are found having large missing transverse energy along a direction opposite in azimuth to that of the high-p_T electron. Both the configuration of the events and their number are consistent with the expectations from the process p̄ + p → W $^\pm$ + anything, with W → e + ν, where W $^\pm$ is the charged Intermediate Vector Boson postulated by the unified electroweak theory.

1. Introduction. The very successful operation of the CERN p̄p Collider at the end of 1982, with peak luminosities of ~5 × 10²⁸ cm⁻² s⁻¹, has allowed the UA2 experiment to collect data corresponding to a total integrated luminosity of ~20 nb⁻¹. According to current expectations [1], these data should contain

approximately four events of the type

$$\bar{p} + p \rightarrow W^\pm + \text{anything}$$
$$\hookrightarrow e^\pm + \nu(\bar{\nu}), \qquad (1)$$

where W$^\pm$ is the charged Intermediate Vector Boson (IVB) which mediates the weak interaction between charged currents [2]. In fact it was the search for such particles, and for the neutral IVB, the Z⁰, that motivated the transformation of the CERN Super Proton Synchrotron (SPS) into a p̄p collider operating at a
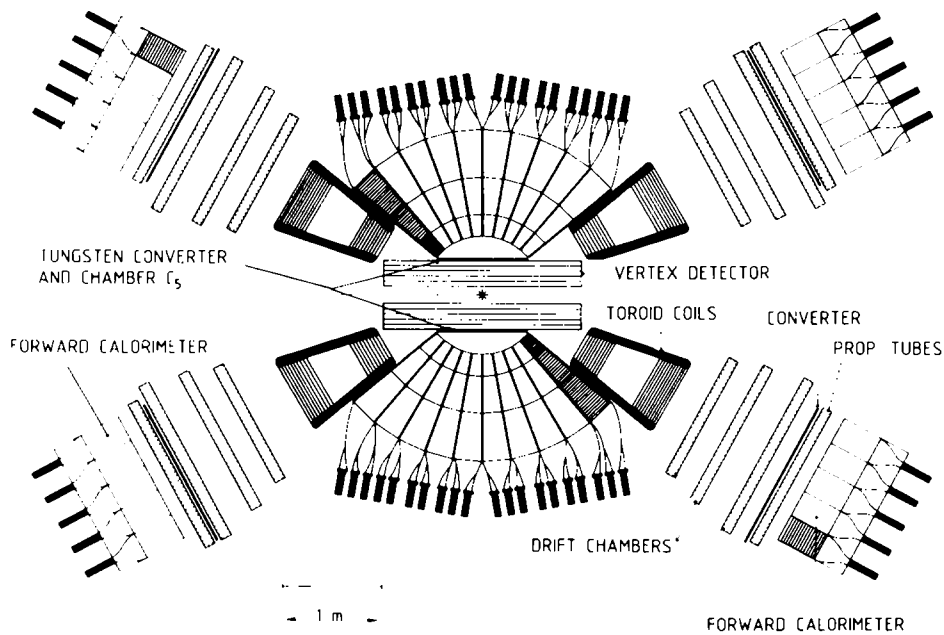
Fig. 1. The UA2 detector: Schematic cross section in the vertical plane containing the beam.

total centre-of-mass energy $\sqrt{s}$ = 540 GeV [3].

We report here the results of a search for single electrons of high transverse momentum (p_T), which are expected to originate from reaction (1). Because the neutrino from W decay is not detected, the events from reaction (1) are expected to show a large missing transverse energy (of the order of the electron p_T) along a direction opposite in azimuth to that of the electron. Results on this subject have been reported earlier [4,5].

The experimental apparatus is shown in fig. 1. At the centre of the apparatus a system of cylindrical chambers (the vertex detector) measures charged particle trajectories in a region without magnetic field. The vertex detector consists of: (a) two drift chambers with measurement of the charge division on a total of 12 wires per track; (b) four multi-wire proportional chambers having cathode strips with pulse height read-out, at ±45° with respect to the wires. These chambers are used to determine the position of the event vertex along the beam line with a precision of ± 1 mm.

The vertex detector is surrounded by a highly segmented electromagnetic and hadronic calorimeter (the central calorimeter), which covers the polar angle in-

terval $40° < \theta < 140°$ and the azimuthal range $30° \leqslant \phi \leqslant 330°$. In the present experiment the remaining azimuthal interval (±30° around the horizontal plane) is covered by a large angle magnetic spectrometer (LAMS), which includes a lead-glass wall, to measure charged and neutral particle production [6] over $\Delta\phi$ = 30°.

The forward regions ($20° < \theta < 37.5°$ and $142.5° < \theta < 160°$, respectively), are each equipped with twelve toroidal magnet sectors, with an average field integral of 0.38 T m, followed successively by: (a) drift chambers; (b) multitube proportional chambers immediately behind a converter to detect showers; (c) electromagnetic calorimeters.

More details on the apparatus will be discussed whenever they are relevant to the present investigation.

2. *Electron search in the central calorimeter.* The central calorimeter is segmented into 200 cells, each covering 15° in ϕ and 10° in θ and built in a tower structure pointing to the centre of the interaction region. The cells are segmented longitudinally into a 17 radiation length thick electromagnetic compartment (lead-scintillator) followed by two hadronic compart-

ments (iron-scintillator) of two absorption lengths each. The light from each compartment is collected by two BBQ-doped light guides on opposite sides of the cell.

All calorimeters have been calibrated in a 10 GeV beam from the CERN PS, using incident electrons and muons. The stability of the calibration has since been monitored using a light flasher system and a ^{60}Co source. The systematic uncertainty in the energy calibration for the data discussed here is less than ±2% for the electromagnetic calorimeter.

The response of the calorimeter to electrons, and single and multi-hadrons, has been measured at the CERN PS and SPS machines using beams from 1 to 70 GeV/c. In particular, both longitudinal and transverse shower development have been studied as well as the effect of particles impinging near the cell boundaries. The energy resolution for electrons is measured to be $\sigma_E/E = 0.14/\sqrt{E}$ (E in GeV). Details of the construction and performance of the calorimeter are reported elsewhere [7].

In the angular region covered by the central calorimeter a cylindrical tungsten converter, 1.5 radiation lengths thick, followed by a cylindrical proportional chamber, is located just after the vertex detector. This chamber, named C_5 (see fig. 1) has cathode strips at ±45° to the wires. We measure the pulse heights on the cathode strips and the charge division on the wires.

In order to implement a trigger sensitive to high-p_T electrons, the gains of the photomultipliers were adjusted so that their signals were proportional to the transverse energy. The eight signals from any 2 × 2 matrix of adjacent electromagnetic cells were then linearly added and their sum was required to exceed a given threshold (typically set at 8 GeV). In order to suppress background from sources other than $\bar{p}p$ collisions, we required a coincidence with two additional signals obtained from scintillator arrays surrounding the vacuum chamber downstream of the interaction point. These arrays were used in an experiment to measure the $\bar{p}p$ total cross section [8]: they gave a coincidence signal in more than 98% of the non-diffractive $\bar{p}p$ collisions.

The full data sample recorded using the W trigger corresponds to a total integrated luminosity of 19.0 nb^{-1}. A first event selection is made by searching for clusters of energy with the configuration expected from isolated electrons. A cluster is obtained by joining all

cells of the electromagnetic calorimeter which share a common side and contain at least 0.5 GeV, and the cluster energy is defined as the sum of all energies contained in the three compartments of both the cluster cells and the surrounding ones. The following requirements are then applied: (i) the cluster must be contained within a 2 × 2 cell matrix; (ii) no more than 10% of the cluster energy must be contained in the electromagnetic compartment of the surrounding cells; (iii) no more than 10% of the cluster energy must be contained in the hadronic compartments; (iv) the cluster centroid must not fall in an edge cell. This last requirement reduces the solid angle acceptance by 25%. Tests with electron beams from the SPS have shown that more than 95% of all isolated electrons in the energy range 10–80 GeV pass the cuts (i) to (iii).

For each cluster satisfying all four requirements a transverse energy E_T' is calculated using the position of the cluster centroid and assuming that the event vertex was in the centre of the apparatus. The events with $E_T' > 15$ GeV (363 events) are fully reconstructed and the exact location of the event vertex (as measured in the vertex detector) is used to obtain the correct value of the transverse energy E_T. The E_T distribution for these events is shown in fig. 2a. The fall-off for $E_T < 17$ GeV results from the selection requirement $E_T' > 15$ GeV applied without knowledge of the exact event vertex. For $E_T > 17$ GeV the distribution of fig. 2a has no threshold bias. There are 7 events with $E_T > 30$ GeV, the highest E_T value being 40.3 GeV.

This sample is further reduced by requiring that one, and only one charged particle track reconstructed in the vertex detector points to the energy cluster. To take the calorimeter cell size into account we define the quantity

$$\Delta^2 = (\delta\theta/10°)^2 + (\delta\phi/15°)^2 , \qquad (2)$$

where $\delta\theta(\delta\phi)$ is the polar (azimuthal) separation between a track and the line joining the event vertex to the cluster centroid. Studies with electron beams from the SPS have shown that $\langle\Delta^2\rangle$ is ~0.13 for high-energy electrons, with 95% having $\Delta^2 < 0.4$. We require that the track with the smallest Δ^2 value has $\Delta^2 < 1$, together with the further condition that no other charged particle track be present in a cone of 10° half-aperture around it. A total of 96 events survive these cuts, with the E_T distribution shown in fig. 2b.
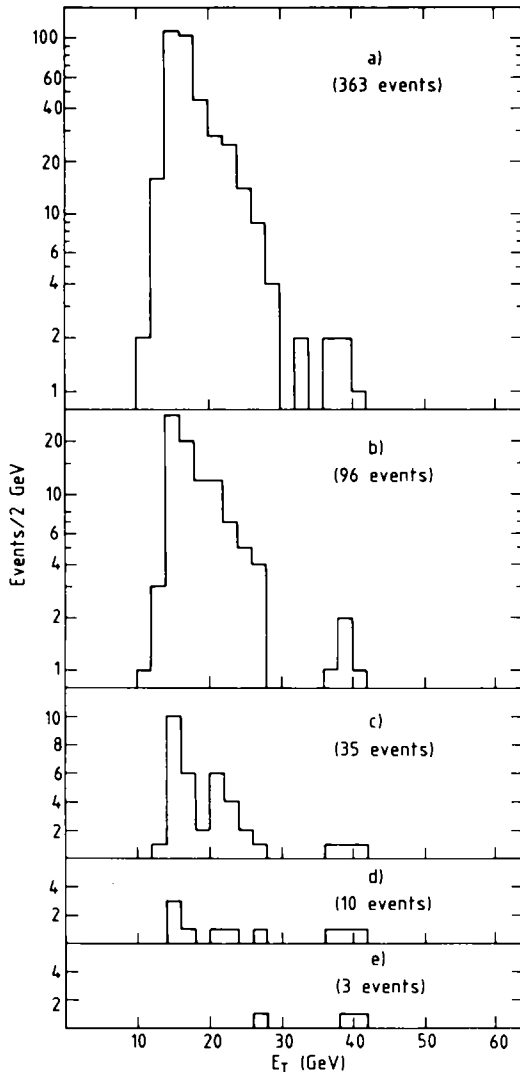
478

Fig. 2. Transverse energy distribution of the event samples in the central calorimeter: (a) After requirements on energy cluster. (b) After association with a track. (c) After association of the track with a shower in the tungsten converter. (d) After requiring only one such shower. (e) After further cuts on the quality of the track-energy cluster matching. This is the final electron sample.

We then require that the track produces a shower in the tungsten converter, with an associated charge cluster in chamber C_5, as expected in the case of electrons. Fig. 3a shows the distribution of d^2, the square of the distance between the track and the closest charge cluster centroid in C_5. Clusters associated with a track
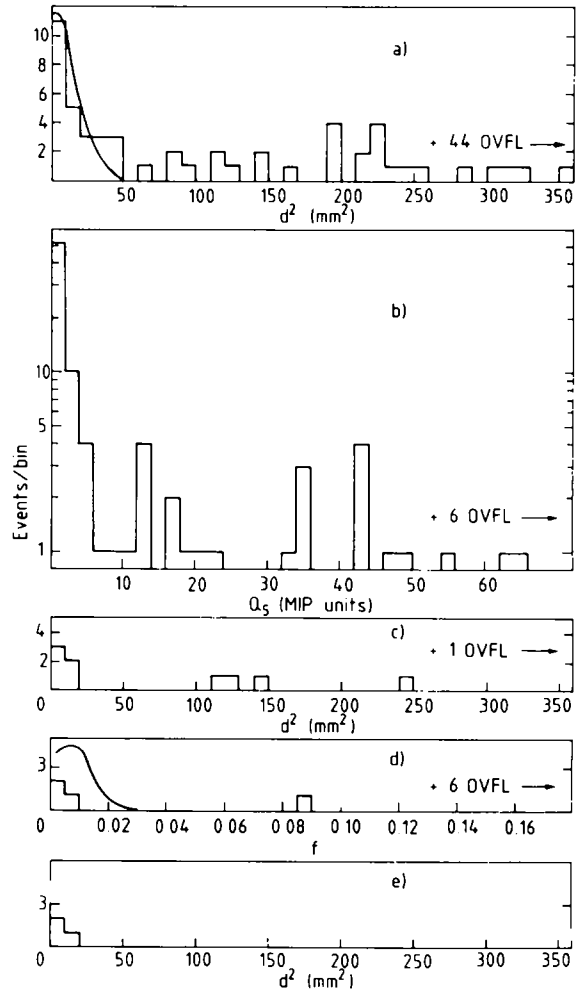

Fig. 3. (a) Distribution of d^2, the distance between the track and the shower in the tungsten converter. The smooth curve represents the distribution measured using high-energy electrons from the SPS (arbitrary normalisation). (b) Distribution of the charge Q_5 (MIP units), observed in chamber C_5 after the tungsten converter. (c) Distribution of d^2 for the sample of 10 events satisfying the isolation criteria. (d) Distribution of f, the quality parameter for the energy cluster shape, as defined in eq. (3). The curve represents the distribution measured using high-energy electrons from the SPS (arbitrary normalisation). (e) Distribution of d^2 for the three electron candidates.

appear as a clear peak superimposed on a flat background.

This background has two origins: (a) chamber C_5 is only ~60% efficient for minimum ionising particles

(MIPs) and whenever the charge cluster generated by a MIP is lost, a cluster not associated with the track is used to calculate d^2: (b) the track-associated cluster may be merged with a nearby cluster (e.g. from photon conversion) and the resulting cluster may have its centroid displaced with respect to the track.

Fig. 3b shows the distribution of Q_5, the charge of the closest cluster with $d^2 < 500$ mm^2, measured in units of the most probable charge generated by a MIP. We have studied the response of chamber C_5 to electrons and pions by exposing a similar device, including a converter and a calorimeter, to a beam from the CERN SPS. In the energy range from ~ 20 to ~ 60 GeV, electron clusters in such a chamber were found to have a broad charge distribution, peaked around $Q_5 \simeq 20$, with more than 90% of the electrons satisfying the condition $Q_5 > 4$. Furthermore, the d^2 distribution of these electrons has $\sigma = 14$ mm^2, with 97% having $d^2 < 50$ mm^2 (see also fig. 3a).

The condition $Q_5 > 4$, when applied to our sample, reduces the number of events from 96 to 35. The E_T-distribution for these events is shown in fig. 2c.

We note that, although the requirement $d^2 < 50$ mm^2 is adequate to select charge clusters associated with electrons, we used the looser cut $d^2 < 500$ mm^2 in order to be able to estimate the background contamination in the final event sample.

In order to further ensure the condition that the electron candidate is isolated, we require that no other charge clusters are present in C_5 in a cone of $10°$ half-aperture around the track. Such clusters could result from the conversion of high-energy photons accompanying the charged particle in the tungsten. We estimate that the loss of events due to radiative corrections [9] is less than 6%.

Ten events satisfy this requirement. The E_T and d^2 distributions for these events are shown in fig. 2d and 3c, respectively.

As a final selection criterion we use the high segmentation of the central calorimeter to check if the shape of the energy cluster is consistent with that expected from an isolated electron impinging along the direction of the observed track. To this purpose we define a quality factor f as follows

$$f = \frac{1}{E}\left(\sum_i (E_i - \widetilde{E}_i)^2\right)^{1/2} , \qquad (3)$$

where E is the measured cluster energy, E_i is the ener-

gy measured in cell i, $\widetilde{E}_i$ is the energy predicted for cell i under the assumption that the observed charged particle track is an electron of energy E, and the sum is extended to all cells of the cluster and those for which $\widetilde{E}_i$ is different from zero. The energies $\widetilde{E}_i$ are obtained from the energy distributions measured in the calorimeter using electron beams from the CERN SPS.

Fig. 3d shows the f distribution for the sample of 10 events. Three events appear to satisfy the condition $f < 0.05$. Such a condition is satisfied by more than 95% of single, isolated electrons, as verified with electron beams from the SPS (see also fig. 3d).

As a further check that the events with $f < 0.05$ are indeed electrons, we estimate the lateral position of the electromagnetic shower in the calorimeter cell from the pulse height ratio of the two photomultipliers and we compare it to the track impact point. We find good agreement (within ±2.5 mm, as expected) for the three events, whereas for the remaining seven events there is a difference of more than 5 mm between these measurements.

The d^2 distribution for the three surviving events is shown in fig. 3e. These events all have $d^2 < 50$ mm^2, as expected for charge clusters in C_5 which are associated with a track. The E_T distribution for these events, which represent our final sample of electron candidates, is shown in fig. 2e.

As a check of this analysis all of the initial sample of 363 events was carefully scanned by physicists using a high resolution graphics terminal. The same three events were found.

There are three main sources of background contamination:

(a) Single, isolated high-p_T π^0- or η-mesons undergoing Dalitz decay, or high-p_T photons (both single and from $\pi^0(\eta) \to \gamma\gamma$ decay) converting in the vacuum chamber wall. Conversions in the detector material were excluded by requiring that the track coordinate were found in at least one of the two innermost chambers of the vertex detector. An upper limit to the number of single π^0- or η-mesons or single photons is obtained from the original sample of 363 events (fig. 2a) by selecting those events with no track pointing to the energy cluster and with at most one charge cluster in chamber C_5 in front of the energy cluster. There are 5 such events with $E_T > 25$ GeV, of which 1 satisfies the requirement $f < 0.05$ [see eq. (3)], as expected

for high-energy isolated π^0- or η-mesons or single photons. Taking into account the probability for photon conversion in the vacuum chamber wall (1.3%) and the Dalitz decay branching ratio, the expected number of background events from this source is <0.04 for $E_T > 25$ GeV.

(b) Single high-p_T charged hadrons interacting in the tungsten converter and depositing a large fraction of their energy (>90%) in the electromagnetic calorimeter. Using high-energy pion beams between 30 and 60 GeV from the CERN SPS we have found that only <1/400 of the pions satisfy these requirements. Assuming that the ratio of charged particles to π^0-mesons at high p_T is 3, we estimate that the expected number of background events from this source is $3/400 \simeq 0.01$ events for $E_T > 25$ GeV.

(c) "Overlap" events, consisting of either at least one high-p_T photon accompanied by a charged particle or of several high-p_T photons of which one converts. In these events the charge cluster observed in chamber C_5 is not correlated with the track, giving rise to a flat background in both d^2 and f variables (see figs. 3c and 3d). Since these variables are correlated, we estimate the overlap background by extrapolating the distribution of the 10 events of figs. 3c and 3d in the d^2, f plane to the region where electrons are expected ($d^2 < 50$ mm^2, $f < 0.05$). This method provides an estimate of 0.6 background events with $E_T > 15$ GeV. Taking into account the E_T distribution of the original event sample (fig. 2a), we estimate this background to be approximately 0.1 event for $E_T > 25$ GeV.

In conclusion, the total background contribution to the three electron candidates amounts to less than 0.2 events for $E_T > 25$ GeV. Furthermore, background sources would have an E_T-distribution similar to that of fig. 2a, whereas the distribution of the three electron candidates is inconsistent with it. This is an independent indication that the background contribution is indeed small.

3. Electron search in the forward detectors. Each of the two forward detectors (see fig. 1) is divided into twelve identical sectors covering 30° in ϕ and 17.5° in θ. A sector consists of:

Three drift chambers located after the magnetic field region. Each chamber consists of three planes, with wires at −7°, 0°, +7°, respectively, with respect to the magnetic field direction.

A 1.4 radiation-lengths thick lead–iron converter, followed by two chambers of proportional tubes (MTPC). Each chamber consists of two layers of 20 mm diameter proportional tubes, staggered by a tube radius and equipped with pulse height measurement. There is a 77° angle between the tubes of the two MTPCs, with the tubes of the first one being parallel to the magnetic field direction. This device localises electromagnetic showers with a precision of ≤ 10 mm, as verified with the data themselves.

An electromagnetic calorimeter consisting of lead-scintillator counters assembled in ten independent cells, each covering 15° in ϕ and 3.5° in θ. Each cell is subdivided into two independent longitudinal sections, 24 and 6 radiation lengths thick, respectively. The light from each section is collected by two BBQ-doped light guides om opposite sides of the cell.

More than 98% of an electron shower is contained in the first section, as verified experimentally up to 80 GeV using electron beams from the CERN SPS. High-energy hadrons, on the contrary, deposit relatively large amounts of energy in the second section which is used, therefore, as a hadron veto. The energy resolution for electrons has been measured to be $\sigma_E/E = 0.15/\sqrt{E}$ (E in GeV). The calibration technique used for these calorimeter modules is similar to that for the central calorimeter.

A trigger sensitive to high-p_T electrons was implemented by requiring that the transverse energy deposited in any 2 × 2 matrix of adjacent cells in the same sector exceed a threshold (typically set at 8 GeV), in coincidence with the small angle scintillator arrays described in section 2. The full data sample recorded with this trigger corresponds to a total integrated luminosity of 16 nb^{-1}.

The forward calorimeter cell size is much larger than the lateral extension of an electromagnetic shower: consequently an electron is expected to deposit its energy in a cluster consisting of at most two adjacent cells. Furthermore, because of the geometry of the calorimeter, these cells must have the same azimuth. A total of 761 events with a cluster transverse energy E_T above 15 GeV has been selected from the full data sample. The E_T distribution of these events is shown in fig. 4a.

We next require that a charged particle track reconstructed in the drift chamber points to the cluster
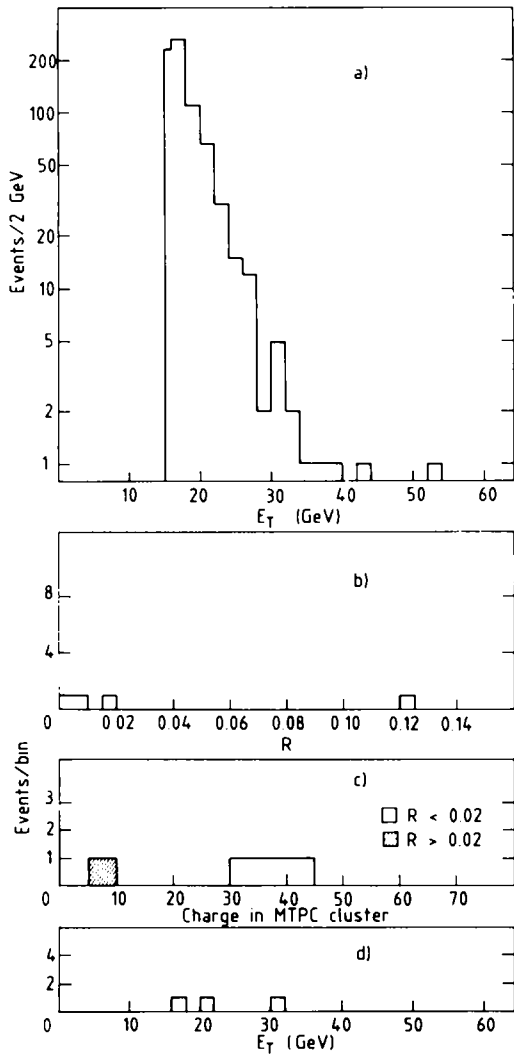
Fig. 4. (a) E_T-distribution of the sample of 761 events selected from energy requirements in the forward calorimeters.
(b) Distribution of R, the ratio between the energy deposited in the hadron veto section of the calorimeter and the cluster energy. (c) Distribution of the charge of the track-associated cluster measured in the MTPCs after the lead–iron converter (MIP units). (d) Transverse energy distribution for the final sample of electron candidates.

centroid. The centroid position along an axis parallel to the magnetic field direction in that sector (the x-axis) is obtained with an accuracy $\sigma = 25$ mm from the pulse height ratio of the two photomultipliers in the cell. We require, therefore, that the x-coordinate

of the track impact point on the calorimeter be within ±70 mm of the cluster centroid.

Because the magnetic field deflects charged particles in the plane defined by the particle direction and the beam line, the track projection in a plane perpendicular to the beam line is required to extrapolate close to the beam axis and to match a track found in the vertex detector within the reconstruction errors. The momentum resolution achieved so far is $\Delta(1/p) = 0.02 \,(\text{GeV}/c)^{-1}$.

We then require that the track matches the position of a shower in the lead- iron converter, as measured by the MTPCs. The distance between the impact point of the track on the MTPCs and the location of the charge cluster in the proportional tubes must not exceed 60 mm in x and 30 mm in the orthogonal coordinate.

The next condition is that the momentum and the shower energy measured in the calorimeter agree within errors. This is done by imposing the condition $|p^{-1} - E^{-1}| < 3\,\sigma$, where σ is obtained by adding in quadrature the contributions of the momentum and energy resolutions quoted above.

In order to further reduce overlap background and to eliminate electrons originating from photon conversions in the vacuum chamber, we require that only one track points to the energy cluster in the calorimeter, and that no additional MTPC cluster is present in front of it. Background due to photon conversions in the detector material is suppressed by requiring the presence of a hit in at least one of the first two chambers in the vertex detector.

In order to ensure that the electron is isolated, we require that the total energy in the calorimeter cells surrounding the energy cluster does not exceed 3 GeV.

Four events survive all these conditions.

The ratio, R, of the energy deposited in the second section of the calorimeter to that deposited in the first section, is shown in fig. 4b. Three events satisfy the electron criterion, $R < 0.02$, whereas one has $R > 0.1$, as expected for hadrons. As a further check, we plot the charge distributions of the clusters measured in the MTPCs for the two classes of events separately (fig. 4c). The large charges associated with the events having $R < 0.02$ are consistent with the behaviour of electrons.

The transverse energy distribution of the electron candidates is shown in fig. 4d.

Backgrounds in this sample are expected to originate from the same sources as described in section 2. However, in this case the background from conversions of high-E_T photons is smaller because the magnetic field separates unresolved e^+e^- pairs.

Concerning the overlap background, we note that soft charged hadrons accompanying high-E_T photons are rejected by the requirement that the measured particle momentum and the energy deposition agree within errors.

The background contribution from high-p_T charged hadrons can be estimated from fig. 4b by extrapolating the distribution of events with $R > 0.02$ to the electron region, $R < 0.02$. There is one event having $R > 0.02$ which we use to estimate that less than 0.2 background events have $E_T > 15$ GeV.

4. Missing transverse momentum. We now verify another feature of reaction (1): namely, the presence of an undetected neutrino with transverse momentum similar in magnitude to that of the electron but opposite in azimuth.

In order to estimate the missing transverse momentum carried away by the neutrino we reconstruct the total momentum vector from the available calorimetric and spectrometric measurements. To each calorimeter cell, including those in the lead glass wall, we assign a vector p_i with magnitude equal to the energy deposited in the cell and direction along the line joining the event vertex to the cell centre. In the forward detectors, when both momentum and the corresponding energy deposition are measured, we use the larger value in order to avoid double counting. The total momentum vector $P = \Sigma_i p_i$ is then projected onto the direction of the electron transverse momentum vector p_{eT} to define the missing transverse momentum P_T^{miss}

$$P_T^{miss} = (P \cdot p_{eT})/E_T , \qquad (4)$$

where $E_T = |p_{eT}|$, and where P includes the electron momentum.

The ratio P_T^{miss}/E_T is shown in fig. 5a for the electron candidates found both in the central calorimeter and in the forward detectors. The events with $P_T^{miss}/E_T \approx 1$ are consistent with reaction (1).

The E_T distribution of the four events with $P_T^{miss}/E_T > 0.8$ is shown in fig. 5b. These electron candidates are those having the highest E_T values.

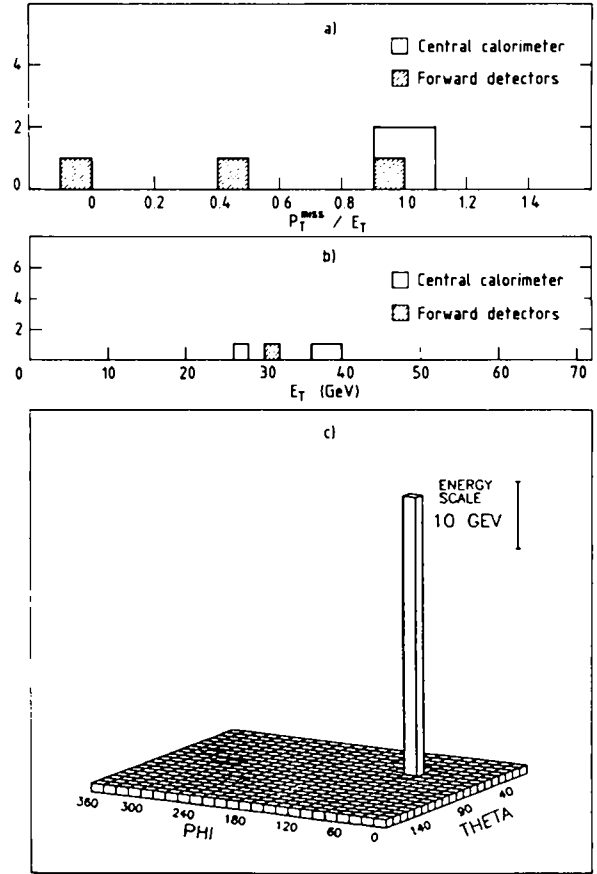The two electron candidates with $P_T^{miss}/E_T < 0.5$

Fig. 5. (a) Distribution of P_T^{miss}/E_T, the ratio between the total missing transverse momentum and the transverse energy of the electron candidate. (b) Transverse energy distribution of the electron candidates observed in events with large missing transverse momentum ($P_T^{miss}/E_T > 0.8$). (c) The cell energy distribution as a function of polar angle θ and azimuth ϕ for the electron candidate with the highest E_T value (event C of table 1).

for which $E_T = 16.3$ and 22.6 GeV, respectively, have both been found in the forward detectors. We note that the isolation criteria used here are looser than those used for the central calorimeter. In particular, we have not applied the condition that no other particle is observed within a 10° half-aperture cone around the electron track, because the higher particle density expected in the angular region of the two forward detectors would reduce the detection efficiency for reaction (1).

Table 1
Parameters of the central calorimeter electrons.

Event	E_T (GeV)	$\frac{E_{had}}{E}$	E_{had2} [a] (GeV)	$\frac{p_T^{miss}}{E_T}$	ΣE_T [b] (GeV)	θ [c] (deg.)	ϕ (deg.)	d (mm)	θ_v (MIPs)	t	Δz [d] (mm)
A	27.7	0.04	0	1.03	13.5	99.7	173.1	12	31	0.003	1.3
B	38.5	0.03	0	0.93	8.5	131.0	248.7	4	95	0.006	-0.7
C	40.3	0.04	0	1.01	4.9	50.2	84.7	6	9	0.002	-2.2

[a] Energy deposited in the second hadronic compartment of the cluster cells.
[b] The sum extends over all particles excepting the electron.
[c] $\theta = 0$ corresponds to the direction of the incident protons.
[d] Distance between the track and the predicted impact in the calorimeter, calculated from the pulse height ratio of the two photomultipliers.

Table 2
Parameters of the forward detector electron with missing transverse momentum.

Event	E_T (GeV)	R	E (GeV)	Electron charge sign	$\frac{p_T^{miss}}{E_T}$	ΣE_T [a] (GeV)	θ [b] (deg.)	ϕ (deg.)	Calorimeter-MTPC match (mm)	Track-MTPC match (mm)	Charge in MTPC (MIPs)
D	30.9	0.004	62.3	+	1.00	15.9	150.3	268.3	68	12	> 38

[a] The sum extends over all particles excepting the electron.
[b] $\theta = 0$ corresponds to the direction of the incident protons.

In order to verify that the large missing transverse momentum of the four electron candidates is not dominated by the limited coverage of the detectors, we have studied a sample of background events obtained from the raw W-trigger sample. This control sample is dominated by events containing a high-E_T jet, which are not expected to show a large missing transverse momentum [10]. We find that the fraction of such events which satisfies the condition P_T^{miss}/E_T > 0.8 is only ~20% for both the central calorimeter and the forward detectors.

A list of relevant parameters for the four events with P_T^{miss}/E_T > 0.8 is given in tables 1,2. For each event the total transverse energy, ΣE_T, of all particles excluding the electron is also shown in tables 1,2. It should be compared with the corresponding value of ~8 GeV for minimum bias events.

Fig. 5c shows the cell energy distribution in θ and ϕ for the highest E_T event (event C in table 1). The only

significant energy flow within the detector acceptance is carried by the electron candidate. The other three events have the same spectacular configuration.

5. *Conclusions.* The application of the various selection criteria used in the analysis to identify single isolated electrons has reduced the original event sample to four events with E_T > 15 GeV and large missing transverse momentum. The number of events, accounting approximately for acceptance and detection efficiency, and their configuration are consistent with expectations from reaction (1).

The assumption that these four electrons indeed originate from the decay $W \rightarrow e\nu$, allows us to estimate the W mass for a given W momentum distribution, assuming W decay kinematics and standard V−A coupling. This is done by fitting the E_T distributions predicted for the four measured θ angles to the measured E_T values.

We find that the best fit value of M_W is rather insensitive to the particular choice of the W momentum distribution, provided that the transverse momentum p_{WT} is much less than $M_W c$. We use gaussian distributions for the three components of the W momentum p_W and vary $(\langle p_{WL}^2 \rangle)^{1/2}$ between 50 and 100 GeV/c, and $\langle p_{WT} \rangle$ between 3 and 8 GeV, where p_{WL} is the longitudinal momentum. The ranges of values used for $(\langle p_{WL}^2 \rangle)^{1/2}$ and $\langle p_{WT} \rangle$ reflect the limits of reasonable production models [1].

The results of the fit gives

$$M_W = (80^{+10}_{-6})\,\text{GeV}/c^2 ,$$

where the quoted error takes into account the effect of varying the W momentum distribution.

This value agrees with the expectation of the electro-weak theory [11].

References

[1] L.B. Okun' and M.B. Voloshin, Nucl. Phys. B120 (1977) 459;
C. Quigg, Rev. Mod. Phys. 94 (1977) 297;
J. Kogut and J. Shigemitsu, Nucl. Phys. B129 (1977) 461;
R.F. Peierls, T. Trueman and L.L. Wang, Phys. Rev. D16 (1977) 1397;
F.E. Paige, BNL 27066 (1979);
F. Rapuano, Lett. Nuovo Cimento 26 (1979) 219;
R. Horgan and M. Jacob, CERN 81 04 (1981) p. 65.

[2] S.L. Glashow, Nucl. Phys. 22 (1961) 579;
S. Weinberg, Phys. Rev. Lett. 19 (1967) 1264;
A. Salam, Proc. 8th Nobel Symp. (Aspenäsgården, 1968) (Almqvist and Wiksell, Stockholm) p. 367.

[3] C. Rubbia, P. Mc Intyre and D. Cline, Proc. Intern. Neutrino Conf. (Aachen, 1976) (Vieweg, Braunschweig, 1977) p. 683;
S. Van der Meer, Stochastic damping of betatron oscillations, CERN/ISR-PO/72–31 (1972).
The Staff of the CERN proton-antiproton project, Phys. Lett. 107B (1981) 306.

[4] M. Banner et al., Preliminary searches for hadron jets and for large transverse momentum electrons at the SPS $\bar{p}p$ Collider, presented Third Topical Workshop on Proton -antiproton collider physics (Rome, January 1983) CERN-EP/83 -23 (1983).

[5] G. Arnison et al., Phys. Lett. 122B (1983) 103;
C. Rubbia, Report Third Topical Workshop on Proton-antiproton collider physics (Rome, January 1983).

[6] M. Banner et al., Phys. Lett. 115B (1982) 59;
M. Banner et al., Phys. Lett. 121B (1983) 187;
M. Banner et al., Phys Lett. 122B (1983) 322.

[7] A.G. Clark, Proc. Intern. Conf. on Instrumentation for colliding beam physics, SLAC-250 (1982);
UA2 Collab., Status and first results from the UA2 experiment, presented 2nd Intern. Conf. on Physics in collisions (Stockholm, June 1982), to be published in Phys. Scr.

[8] R. Battiston et al., Phys. Lett. 117B (1982) 126.

[9] E. Calva-Tellez et al., Lett. Nuovo Cimento 4 (1972) 619.

[10] M. Banner et al., Phys. Lett. 118B (1982) 203.

[11] For a review see: J. Ellis et al., Ann. Rev. Nucl. Part. Sci. 32(1982) 443.